Photoelectron spectroscopy and inferred femtosecond intramolecular dynamics of $C_2H_2^+$ and $C_2D_2^+$

J. E. Reutt, L. S. Wang, J. E. Pollard,[a] D. J. Trevor,[b] Y. T. Lee, and D. A. Shirley
Materials and Molecular Research Division, Lawrence Berkeley Laboratory and Department of Chemistry, University of California, Berkeley, California 94720

(Received 25 November 1985; accepted 12 December 1985)

The 584 Å photoelectron spectra of rotationally cold C_2H_2 and C_2D_2 were obtained with improved resolution, permitting the first three electronic states of the ions to be characterized in greater detail. Temperature-dependent studies led to a definitive assignment of the low intensity features in the $\tilde{X}\,^2\Pi_u$ state, yielding $\nu_4 = 837 \pm 12\ cm^{-1}$ for $C_2H_2^+$ and $\nu_4 = 702 \pm 12\ cm^{-1}$ for $C_2D_2^+$. The ν_5 origin of the Renner–Teller multiplet was identified. In the case of $C_2D_2^+$, a Fermi resonance with this multiplet contributed intensity to the ν_1 mode, facilitating its evaluation at $2572 \pm 16\ cm^{-1}$. The C_{2h} geometry of the $\tilde{A}\,^2A_g$ state was determined from the two previously unobserved bending progressions, assigned to ν_4 and ν_{5B}, and evaluated at 492 ± 12 and $605 \pm 12\ cm^{-1}$ for $C_2H_2^+$ and 339 ± 12 and $516 \pm 12\ cm^{-1}$ for $C_2D_2^+$, respectively. A more extensive vibrational progression than previously evident, comprised of irregular spectral features indicative of nonadiabatic effects, was observed for the $B\,^2\Sigma_u^+$ state. Autocorrelation functions were derived from the spectra for all three electronic states, and the two electronically excited states exhibit an ultrafast decay on a 10^{-14} s time scale. The $\tilde{A}\,^2A_g$ state decays within one period of bending vibration, while the $\tilde{B}\,^2\Sigma_u^+$ state survives only 14 fs, corresponding to a single period of symmetric stretching motion.

I. INTRODUCTION

The nonresonant photoionization process associated with HeI photoelectron spectroscopy typically produces ions with 0–15 eV internal energies. The electronically and vibrationally excited ions are subject to relaxation processes. In cases where ultrafast (10^{-14} s) nonradiative relaxation occurs from the initially formed states, the vibrational fine structure in the photoelectron spectra will become diffuse. Such photoelectron bands then provide information concerning both the initially formed states and the dynamics of these states.

The intramolecular dynamics of the acetylene ion and its deuterated analog might be expected to exhibit characteristics intermediate between those of very small molecules and those of larger polyatomics. Because of its intermediate size, the central question in both the relaxation and decomposition of the excited-state ion is whether the density of background vibrational levels and electronic states is sufficient to serve as a quasicontinuum in the intramolecular relaxation process. Or, failing this, are there particular doorway states involved in the decay, determining the relaxation pathways and rates? We have addressed these questions experimentally by performing high resolution photoelectron spectroscopy on supersonic molecular beams of C_2H_2 and C_2D_2 deriving autocorrelation functions from the spectra.

Through the Heisenberg uncertainty relationship and under the Born–Oppenheimer approximation, Heller has shown that the time evolution of the initially formed wave packet, described by an autocorrelation function, may be obtained through an appropriate Fourier transform of the absorption spectrum.[1] This method has been used to obtain autocorrelation functions from the photoelectron spectra of N_2^+, HBr^+, HCN^+, and $C_2H_4^+$.[2,3] These autocorrelation functions describe the vibrational wave packet as it propagates on the upper potential energy surface. The usefulness of this approach in interpreting complex spectra is illustrated for electronically excited states of HCN^+ and $C_2H_4^+$. The correlation functions exhibit rapid decay that is indicative of a fast intramolecular energy transfer. Caution must be exercised in extracting quantitative results from these experimentally derived correlation functions, however, because the initially formed wave packet is not a single eigenstate of the system, but rather a coherent superposition of eigenstates of all ionic states accessible with the irradiating photons.[4] Although this prevents the correlation function from being rigorously quantitative, the time scale of the nonradiative decay will be manifested in the experimentally derived correlation functions.

Numerous investigations of the spectroscopy, photoionization, and subsequent behavior of the acetylene ion in each of the three electronic states accessible with HeI (21.218 eV) photons have resulted in a partially characterized ground $^2\Pi_u$ electronic state and less complete descriptions of the excited $\tilde{A}\,^2\Sigma_g^+$ and $\tilde{B}\,^2\Sigma_u^+$ states. (Here the traditional term symbols, applied under an assumed $D_{\infty h}$ symmetry, are used to represent the electronic states.) Early photoelectron spectroscopy studies by Baker and Turner revealed a very short progression in the ν_2, predominantly C–C stretching, mode of the ground $^2\Pi_u$ state.[5] A complex band was reported for the first excited $^2\Sigma_g^+$ state, and a vibrational assignment of the spectra, as combination bands of the ν_2 and ν_1 modes,

[a] Present address: The Aerospace Corporation, M21253, P.O. Box 92957, Los Angeles, CA 90009.
[b] Present address: Exxon Research and Engineering Company, Annandale, NJ 08801.

 0021-9606/86/063022-10$02.10

was proposed for $C_2D_2^+$ only. The second excited $^2\Sigma_u^+$ state of each ion exhibited vibrational structure also assigned as combinations of the ν_2 and ν_1 modes. More recently reported photoelectron spectra have not provided additional information about the vibrational fine structure in the excited electronic states.[6,7] Dehmer and Dehmer[7] reported a spectrum of the ground state of $C_2H_2^+$, which manifested low intensity features in addition to the previously observed ν_2 progression, and attributed these to unspecified ν_4 and ν_5 Renner–Teller active bending modes.

Photoionization efficiency curves for $C_2H_2^+$ and the fragment ions from C_2H_2 have been reported over the 400–1100[8] and 600–1000 Å[9] regions. For the parent-ion curve, two broad maxima centered at 930 and 810 Å with some additional structure are observed below the second ionization threshold and are assigned to autoionizing states of acetylene. The photoionization threshold for C_2H^+ formation was reported by Dibeler, Walker, and McCulloh at 17.36 ± 0.01 eV, placing it approximately 1.0 eV above the adiabatic ionization potential for the $\tilde{A}\,^2\Sigma_g^+$ state and about 0.5 eV greater than the value determined for the thermochemical threshold.[10] Two more recent studies of the C_2H^+ photoionization threshold, however, report a low intensity onset in C_2H^+ formation occurring at 16.79 ± 0.03 eV, followed by a large increase in formation at 17.36 eV.[8,11] Although these latter studies have resolved the discrepancy between values for the thermochemical and photoionization appearance potentials, they do not explain the delay of 0.5 eV before an appreciable amount of C_2H^+ is formed, and the value for the thermochemical appearance potential itself may contain substantial error. The appearance potentials of C_2^+ (19.4 eV) and CH^+ (20.7 eV) fall above threshold for the $\tilde{B}\,^2\Sigma_u^+$ state. At a photon energy of 21.218 eV, however, the predominant ions formed (>98%) are $C_2H_2^+$ and C_2H^+.[8]

The subsequent behavior of excited state $C_2H_2^+$ has been investigated by photoelectron–photoion and photoelectron–photon coincidence methods as well as by several theoretical approaches. Both coincidence studies employed 21.218 eV photons. The photoelectron–photoion study revealed formation of C_2H^+ from levels of the $\tilde{A}\,^2\Sigma_g^+$ state above 17.3 eV, but no C_2H^+ below this energy, in agreement with the earliest PIE work.[12] At 17.6 eV anomalous peak shapes suggested a reappearance of the parent ion from the $\tilde{A}\,^2\Sigma_g^+$ state and incomplete predissociation of this state. Yet no $C_2H_2^+$ $\tilde{A} \rightarrow \tilde{X}$ emission was detected in the photoelectron–photon coincidence measurement.[13] Quasiequilibrium theory (QET) calculations indicated that the electronic excitation energy of the acetylene ion is generally, *but not completely*, randomized.[14] The $\tilde{A}\,^2\Sigma_g^+$ state relaxation does not, therefore, occur through complete internal conversion or through radiative decay to the $\tilde{X}\,^2\Pi_u$ state.

Beginning with C_2 and introducing a single proton to obtain multiplicity, spins, and symmetries, Fiquet-Fayard utilized known correlation rules and energetics to determine asymptotic limits (in parentheses) for the $\tilde{X}\,^2\Pi_u$ ($^3\Pi_u$) and $\tilde{A}\,^2\Sigma_g^+$ ($^1\Sigma_g^+$) states.[15] She noted that the $^2\Sigma_g^+$ potential energy surface could cross with a repulsive $^4\Sigma_g^-$ surface, but that the energetics probably prevented a surface crossing. Her calculations placed the $^4\Sigma_g^-$ surface completely below the $^2\Sigma_g^+$ surface, thereby eliminating this predissociation mechanism and leaving no mechanism for the relaxation of the $\tilde{A}\,^2\Sigma_g^+$ state. The $\tilde{B}\,^2\Sigma_u^+$ state, on the other hand, does have a curve crossing with a repulsive $^4\Pi_u$ state. Complete predissociation was predicted to occur from the $\tilde{B}\,^2\Sigma_u^+$ state via spin-orbit coupling to the $^4\Pi_u$ state.

Rosmus, Botschwina, and Maier have demonstrated with *ab initio* self-consistent field (SCF) and pseudonatural orbital-coupled electron pair approximation (PNO–CEPA) calculations that a unimolecular arrangement of the $C_2H_2^+$ $\tilde{A}\,^2\Sigma_g^+$ state to the $\tilde{A}\,^2A_1$ state of H_2CC^+ (vinylidenic structure) may contribute to the nonradiative decay.[16] Their calculations indicate that the ν_4 (π_g) bending mode initiates a reaction pathway with virtually no energy barrier, leading to the $\tilde{B}\,^2B_2$ state of $H_2C_2^+$ (vinylidenic structure). This pathway avoids a curve crossing with the $\tilde{A}\,^2A_1$ state of the vinylidene ion, giving rise to the possibility for further decay. Their results also verify that the repulsive $^4\Sigma_g^-$ $C_2H_2^+$ state lies completely below the $^2\Sigma_g^+$ state, but is positioned for possible interaction with the more accessible vinylidenic states.

In this work HeI (21.218 eV) photoelectron spectra were obtained from supersonic molecular beams of C_2H_2 and C_2D_2. Rotationally cold samples and improved resolution have elucidated additional structure in the spectra of each of the three electronic states. Refined or previously unmeasured spectroscopic constants are reported and the applicability of the normal mode description is discussed. Correlation functions are derived for each isotope and ultrafast decay mechanisms are observed for the two excited electronic states of each species. Section II of this paper contains the details of the experiment. An abbreviated derivation and the method for calculating the autocorrelation functions from the experimental data are presented in Sec. III. The

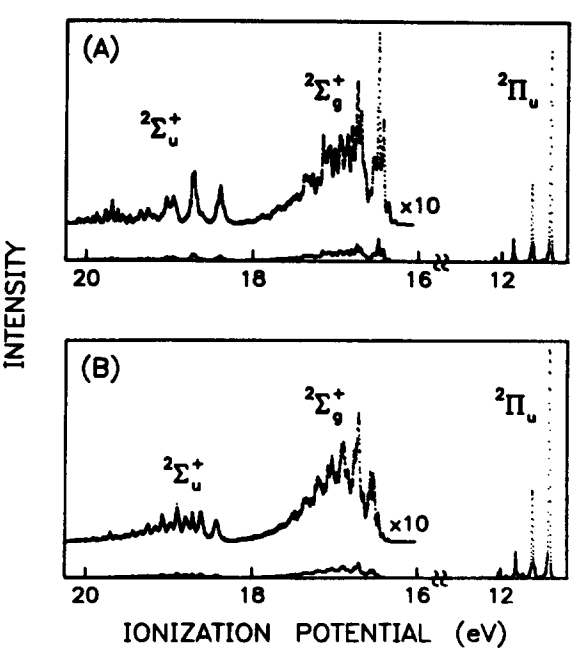

FIG. 1. The HeI (584 Å) photoelectron spectra of C_2H_2 (A) and C_2D_2 (B). The states are labeled with an assumed $D_{\infty h}$ symmetry.

spectroscopy and intramolecular dynamics of $C_2H_2^+$ and $C_2D_2^+$ are presented and discussed in detail in Sec. IV. The principal conclusions are summarized in Sec. V.

II. EXPERIMENTAL

The complete photoelectron spectra of acetylene and dideuterated acetylene, displayed in Fig. 1, were obtained with a resolution of 12 meV FWHM, as measured for Ar $^2P_{3/2}$. The molecular beam photoelectron spectrometer, consisting of a 90° spherical sector prefilter, a 180° hemispherical analyzer, associated electron optics, and multichannel detection, has been described in detail.[17] The electrons are collected at a 90° angle with respect to the incident photon beam and the supersonic molecular beam and the intensity is uncorrected for angular distribution effects. Acetylene β values for HeI photons are available for the $\tilde{X}\,^2\Pi_u$ and $\tilde{A}\,^2\Sigma_g^+$ states and are 1 and 0.3, respectively,[18] yielding a 1.16:1.0 preference for collection of $^2\Sigma_g^+$ electrons to $^2\Pi_u$ electrons for the nonpolarized radiation employed here. No β value was found in the literature for the $\tilde{B}\,^2\Sigma_u^+$ state.

Acetylene of 99.6% purity was obtained from Matheson. It was passed through a dry ice/ethanol trap at 900 Torr and expanded through a 70 μm diam nozzle at room temperature. The molecular beam was characterized with 584 Å photoionization and a quadrupole mass filter (Extranuclear Laboratories). Under these conditions the presence of $< 1\%$ clusters was observed. Additional photoelectron spectra were taken at nozzle temperatures of -62, 120, and 360 °C, in order to identify hot band contributions. Spectra obtained with harder beam expansion conditions (1600 Torr neat acetylene and 1600 Torr 2% acetylene seeded in helium) provided no additional line narrowing.

The deuterated acetylene was prepared by addition of D_2O (99.8% purity Aldrich) under vacuum to calcium carbide (80% purity Alfa products). Impurities were removed by passing the C_2D_2 through a dry ice/ethanol trap before it was expanded at a stagnation pressure of 500 Torr through a 70 μm diam nozzle at room temperature.

The complete photoelectron spectrum of each isotopic species was obtained as four sequential scans of the electron kinetic energy. Each scan was preceded and immediately followed by an argon calibration scan. In order to improve the statistics, four complete spectra of C_2H_2 were obtained and summed. The scan width was determined by measuring the voltage of the power supply controlling the kinetic energy with a computer-interfaced precision digital voltmeter (Dana 5900) at four points during the scan. The linearity of the kinetic energy scale was determined by obtaining the N_2^+ photoelectron spectrum and comparing the N_2^+ $\tilde{X}\,^2\Sigma_g^+$ ($v = 0$) and $\tilde{B}\,^2\Sigma_u^+$ ($v = 0$) splitting with the accurate literature value (3.16981 eV) obtained from optical emission spectroscopy.[19] At higher kinetic energies, the linearity of the energy scale was determined from photoelectron spectra obtained from xenon and argon. The ionization potentials of these rare gases (Ar $^2P_{3/2} = 15.759\,75$ eV and Xe $^2P_{3/2} = 12.130\,00$ eV) have been accurately determined from optical spectroscopy.[20] The molecular beam photoelectron spectrometer maintains an energy scale linear to within ± 0.001 eV over this entire energy range.

An additional source of error resulted from a drift in the energy scale of $\leqslant 0.002$ eV over a 2 h period. This was attributed to C_2H_2- and C_2D_2-induced modification of the surface potentials in the photoelectron spectrometer. This error was minimized by limiting individual scan lengths to 2 h and frequently recalibrating the energy scale with rare gases. The systematic error arising from the small nonlinearity and drift in the energy scale limits the accuracy of the absolute values of the reported ionization potentials to ± 0.005 eV. Other spectroscopic constants are obtained from line splittings, thereby reducing the systematic error, and may be reported to higher accuracies.

III. THE CORRELATION FUNCTION

Correlation functions determined from photoelectron spectra allow one to infer intramolecular dynamics of molecular ions on an ultrafast (femtosecond) time scale. A variety of unimolecular decay processes such as direct dissociation, predissociation, nonradiative transitions, and fluorescence, are available to excited state ions and of these the first three processes tend to occur on time scales commensurate with the correlation function. Although it would be preferable to have real-time femtosecond measurements of the decay of a single prepared eigenstate of the excited state ion, this is not experimentally feasible. Through autocorrelation functions one can extract qualitative, albeit limited, information about dynamics on a femtosecond time scale. Meaningful interpretations of the correlation functions, however, require complementary information available from theoretical calculations of the initial and nearby interacting potential energy surfaces, as well as experimentally determined details of the photofragments and fluorescence produced from the initially formed electronic state.

The time scale for which the correlation function is reliable is determined by both the instrumental resolution, typically 11–12 meV for our apparatus as measured with argon, and the ability to deconvolute the instrument response function to provide an effective resolution. In the present experiment, an effective resolution of 3 meV leads to a time window of greater than 200 fs. Within this window, the time resolution is determined by the width of the photoelectron band of interest. A typical width of 1 eV corresponds to a resolution of a fraction of a femtosecond.

The correlation function can be expressed as

$$C(t) = |\langle \phi(0) | \phi(t) \rangle|, \tag{1}$$

where $C(t)$ is the probability amplitude at time t that the system remains in the initially prepared system and ϕ is the nuclear wave function of the wave packet produced on the upper potential energy surface. This can be extracted from the photoelectron spectrum from the following argument, which has been previously applied to the analysis of the ethylene photoelectron spectrum.[3] The form for the photoionization cross section within the strict Franck–Condon approximation is given by[21]

$$\sigma(E) \propto M_{ei}(R,E)^2 |\langle \psi'' | \psi' \rangle|^2, \tag{2}$$

where $M_{ei}(R,E)$ is the pure electronic transition moment, a function of the nuclear coordinates (R) and the electrons' kinetic energies (E), and ψ'' and ψ' are the initial- and final-

state vibrational wave functions. The electronic transition moment is not expected to vary significantly over the photoelectron band and a constant value is therefore employed. By applying the completeness relation to the set of eigenstates ψ'' of a molecular Hamiltonian and invoking the analytical expression for the Dirac δ function it has been shown[2] that the form of the cross section becomes

$$\sigma(E) \propto (1/2\pi)\int_{-\infty}^{+\infty} e^{iEt/\hbar}\langle\psi''|e^{-iEt/\hbar}|\psi''\rangle\, dt. \qquad (3)$$

In this expression ψ'' is identified as the initial nuclear wave function, $\phi(0)$, and $e^{-iEt/\hbar}|\psi''$ as $\phi(t)$. Making these substitutions results in

$$\phi(E) \propto (1/2\pi)\int_{-\infty}^{+\infty} e^{iEt/\hbar}\langle\phi(0)|\phi(t)\rangle\, dt. \qquad (4)$$

Finally, by a Fourier transform of the cross section one obtains

$$C(t) = |\langle\phi(0)|\phi(t)\rangle| \propto \int_{-\infty}^{+\infty} \sigma(E)e^{-iEt/\hbar}\, dE. \qquad (5)$$

In order to evaluate the correlation function, we need first to determine $\sigma(E)$ from the quantity $I(E)$, intensity vs energy, which we measure. This is achieved by deconvoluting the instrument response function, which we determine from the photoelectron spectrum of a rare gas at a kinetic energy comparable to the band of interest. In this experiment the Ar $^2P_{3/2}$ line was used exclusively.

The ground $^2\Pi_u$ state of $C_2H_2^+$ and $C_2D_2^+$ possesses a small spin-orbit splitting, which introduces an oscillatory factor in the correlation function. This effect is removed by dividing the correlation function by $|\cos(\Omega t/2\hbar)|$, as suggested by Lorquet, Lorquet, Delwiche, and Hubin-Franskin.[2] A value of 4 meV (32 cm^{-1}) was selected for Ω, the spin-orbit splitting, because it was comparable to the estimated value[22] of 50 cm^{-1} and provided an overall monotonic behavior for the ground state correlation function. The 50 cm^{-1} value appears to be too high, since it creates greater than unity values for the correlation function at longer times. To ensure a pure vibrational correlation function, we have also found it necessary to convolute the instrument response with a narrow Gaussian to account for a residual rotational temperature present in the sample following the supersonic expansion. A Gaussian of 2 meV FWHM was determined from the $\tilde{X}\,^2\Pi_u$ state by optimizing the correlation function to maintain an overall monotonic slope.

The correlation functions for the $\tilde{X}$, $\tilde{A}$, and $\tilde{B}$ states of $C_2H_2^+$ and $C_2D_2^+$ were determined by the following method. Each photoelectron band was isolated and the empirically determined background, plus any constant background, was removed. The resulting band was normalized, yielding $I(E)$, and then transformed using a discreet fast Fourier transform. The combined effect of the instrument response function and residual rotational broadening was then removed. This was achieved by dividing the product of separate fast Fourier transforms of the normalized argon spectrum [designated $I_{Ar}(E)$] and a normalized Gaussian of 2 meV FWHM [designated $g(E)$] into the Fourier transformed photoelectron band. The modulus of the quotient was then evaluated, resulting in the autocorrelation function. For the $\tilde{X}\,^2\Pi_u$ state only, the final correction for the spin-orbit splitting was then applied. The procedure is summarized below:

$$C^{vib}(t) = \frac{1}{|\cos(\Omega t/2\hbar)|}\left|\int_{-\infty}^{+\infty} I(E)e^{-iEt/\hbar}\, dE \Big/ \left[\int_{-\infty}^{+\infty} I_{Ar}(E)e^{-iEt/\hbar}\, dE \times \int_{-\infty}^{+\infty} g(E)e^{-iEt/\hbar} dE\right]\right|. \qquad (6)$$

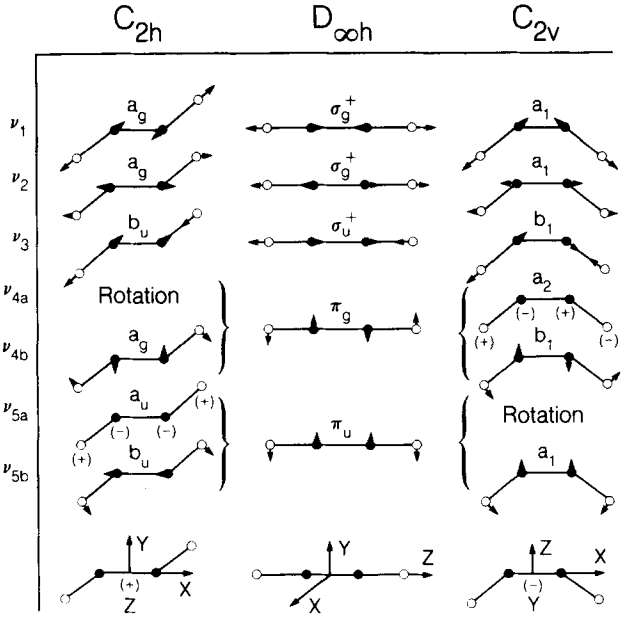

FIG. 2. Normal modes of vibration of an X_2Y_2 molecule in the *trans*-bent C_{2h}, linear $D_{\infty h}$, and *cis*-bent C_{2v} configurations.

Several effects arising from the coherent distribution of states present in the initially formed wave packet contribute to the appearance of the correlation function. In addition to the dynamical processes of interest there are effects due to vibrational anharmonicity and to the phase relationship between the oscillators in a multimode system. The net effect of vibrational anharmonicity is to damp the correlation function, by creating a phase randomization at longer times. Since most physical systems contain a measurable degree of anharmonicity, the experimental correlation functions will display such damping. For example, the $\tilde{X}\,^2\Sigma_g^+$, $\tilde{A}\,^2\Pi_u$, and $\tilde{B}\,^2\Sigma_u^+$ states of N_2^+ exhibit anharmonicities of 16.10, 15.02, and 23.18 cm^{-1}, respectively,[23] and maintain correlations in excess of 0.85 at times greater than 100 fs.[2] This provides a reference for the magnitude of correlation losses due to anharmonicity.

The presence of more than one mode produces a more complex effect on the correlation function. A beat pattern will be introduced by the relative phases of the modes of vibration. The structure of this beat pattern will be determined both by the relative frequencies of the vibrations and by the relative population of the modes. The time scale on which the beat pattern and associated damping occurs must not be mistaken for the time scale on which the dynamical processes of interest occur.

TABLE I. Spectroscopic constants for $C_2H_2^+$ and $C_2D_2^+$.

State		Adiabatic I.P. (eV)	Vibrational frequencies (cm^{-1}) ν_1	ν_2	ν_3	ν_4	ν_5
$C_2H_2^+$							
$\tilde{X}\,^2\Pi_u$							
	This work	11.403(5)		1829.0(2.5)[a]		837(12)	
	Ref. 7	11.406(5)		1807			
	Ref. 6	11.43					
	Ref. 5	11.40		1830			
	Ref. 10	11.402(5)					
$\tilde{A}\,^2A_g$							
	This work	16.297(5)	2530(20)	1730(20)		492(12)	605(12)
	Ref. 6	16.76					
	Ref. 5	16.36					
$\tilde{B}\,^2\Sigma_u^+$							
	This work	18.391(5)	1815(20)	2500(20)			
	Ref. 6	18.71					
	Ref. 5	18.38	1900	2510			
$C_2D_2^+$							
$\tilde{X}\,^2\Pi_u$							
	This work	11.405(5)	2572(16)	1651(4)[b]		702(12)	
	Ref. 5	11.40		1610			
	Ref. 10	11.408(5)					
$\tilde{A}\,^2A_g$							
	This work	16.351(5)	2280(20)	1450(20)		339(12)	516(12)
	Ref. 5	16.53	2500	1370			
$\tilde{B}\,^2\Sigma_u^+$							
	This work	18.427(5)	1475(20)	2275(20)			
	Ref. 5	18.44	1420	2290			

[a] $\omega_e x_e = 6.0 \pm 0.8\ cm^{-1}$.
[b] $\omega_e x_e = 5.6 \pm 0.8\ cm^{-1}$.

The consequence of the vibrational anharmonicity and beat pattern is that the slope of $\ln\{[C(t)]^2\}$ cannot exactly measure the nonradiative decay time. In the case of ultrafast decay, however, the extensive loss of correlation will be recognizable beyond any smaller losses originating from the composition of the Franck–Condon ensemble itself. A significant loss of correlation can thus be related to dynamical processes, and can yield time scales on which those processes occur.

IV. RESULTS AND DISCUSSION

Results for the first three electronic states of $C_2H_2^+$ and $C_2D_2^+$ are discussed separately below. The vibrational normal modes of an X_2Y_2 molecule are illustrated in Fig. 2. Table I presents a summary of our measured spectroscopic constants, together with those previously available in the literature.

A. $\tilde{X}\,^2\Pi_u$ state

Spectra of the ground electronic state of $C_2H_2^+$ and $C_2D_2^+$ taken at 297 K are displayed in Fig. 3. The $\tilde{X}\,^2\Pi_u$ ν_2 progression is described by vibrational and anharmonicity constants of $\nu_2 = 1829.0 \pm 2.5\ cm^{-1}$ and $\omega_e x_e = 6.0 \pm 0.8\ cm^{-1}$ for $C_2H_2^+$ and $\nu_2 = 1651 \pm 4\ cm^{-1}$ and $\omega_e x_e = 5.6 \pm 0.8\ cm^{-1}$ for $C_2D_2^+$. These constants were obtained through a linear regression of the centroids of the four principal peaks, which are averages of the unresolved spin-orbit split states. Linewidths of 16 meV FWHM indicate a spin-orbit splitting of $32 \pm 8\ cm^{-1}$, and correction for this spin-orbit splitting leads to adiabatic thresholds of 11.403(5) eV for $C_2H_2^+$ and 11.405(5) eV for $C_2D_2^+$. [Errors are reported parenthetically, in units of the last digit; i.e., 11.403(5) eV corresponds to 11.403 ± 0.005 eV.]

The lower intensity features of the ground state, labeled a–c, were examined as functions of temperature in order to assess the hot-band contributions. Only the features labeled a, appearing as high ionization potential shoulders on the main ν_2 progression, result solely from hot band contributions. These features are shifted up in energy by 0.031(3) and 0.028(3) eV from the principal peaks of the $C_2H_2^+$ and $C_2D_2^+$ spectra, respectively. This indicates the hot mode is of a higher frequency in the ion than in the neutral molecule. The features designated c, occurring at 0.207(2) and 0.174(2) eV higher binding energies than the $[0\nu_2000]$ levels of $C_2H_2^+$ and $C_2D_2^+$, respectively, are too low in frequency to correspond to stretching modes and must be attributed to two quanta of bending excitation. (Here $[0\nu_2000]$ refers to peaks originating from the transtition $0\nu_2000 \leftarrow 00000$.) This yields bending frequencies of 837(12) cm^{-1} for $C_2H_2^+$ and 702(12) cm^{-1} for $C_2D_2^+$. These bending frequencies are each 226 cm^{-1} (28 meV) higher than the neutral molecule's ν_4 mode, identifying the spectral hot features, a, as $[0\nu_2010] \leftarrow [00010]$ transitions. Since the ν_4 mode is

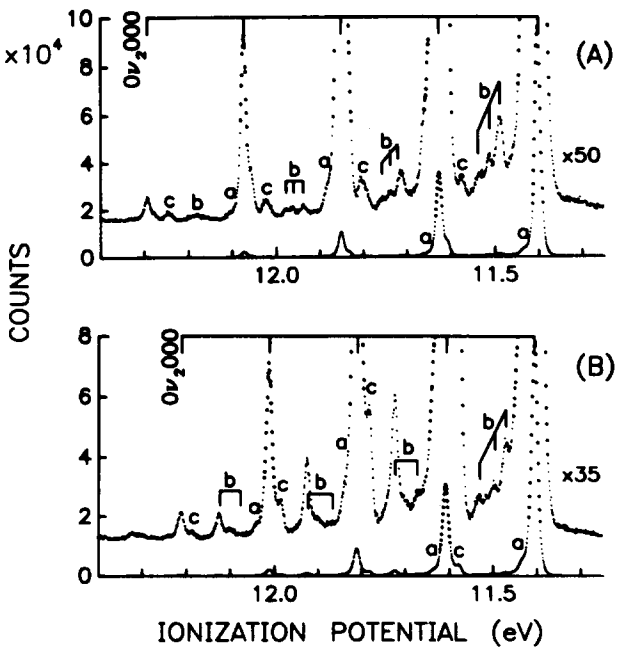

FIG. 3. The $\tilde{X}\,^2\Pi_u$ state photoelectron bands of C_2H_2 (A) and C_2D_2 (B). The features labeled "a" arise from hot band contributions. A Renner–Teller multiplet is assigned to feature "b." Two quanta of ν_4 vibration in combination with the ν_2 mode appear as feature "c."

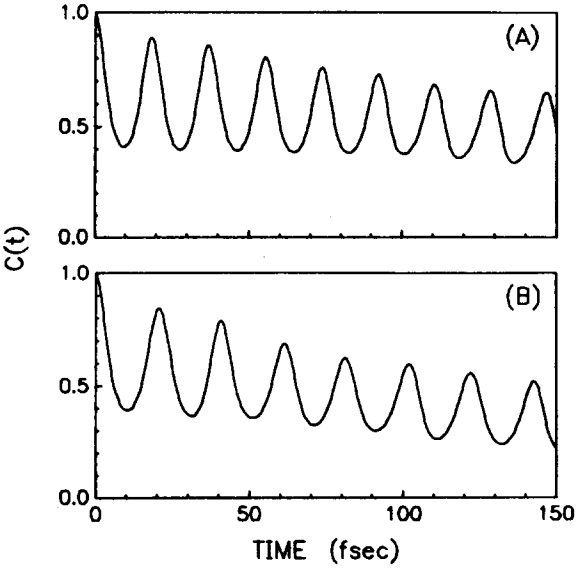

FIG. 4. The correlation functions calculated for the $\tilde{X}\,^2\Pi_u$ state of $C_2H_2^+$ (A) and $C_2D_2^+$ (B).

prominent in the cold spectra in units of two quanta only, this mode does not couple strongly to the $^2\Pi_u$ electronic state and undergo an appreciable Renner–Teller type distortion.

The multiplet features labeled b, present in combination with the ν_2 progression are assigned to a Renner–Teller multiplet arising from interaction of the remaining doubly degenerate *cis* bending mode ν_5 and the $^2\Pi_u$ electronic state. The Renner–Teller interaction of a singlet Π state for linear X_2Y_2 molecules has been treated theoretically by Petelin and Kiselev.[24] They give the following form for the vibronic levels of the molecule with one quantum of ν_5 bending excitation:

$$G(v,0) = \omega_5[1 - (1/8)\epsilon_2^2 \pm (1/2)\epsilon_2](v_5 + 1) + \omega_4[1 - (1/4)\epsilon_1^2] \quad (7)$$

when $K = 0$ and

$$G(v,K) = \omega_5[(v_5 + 1)] - (1/8)\epsilon_2^2 K(K+1) + \omega_4[1 - (1/4)\epsilon_1^2] \quad (8)$$

when $K \neq 0$ and $v = K - 1$. Here ϵ_1 and ϵ_2 are the Renner–Teller constants for the ν_4 and ν_5 modes, respectively. In the present case, spin-orbit interactions should cause a further shifting and splitting of the three vibronic levels described above for the singlet state with one quantum of bending excitation. Because we can resolve only three spectral features, however, the magnitude of the effects due to spin-orbit coupling are apparently smaller than those due to the Renner–Teller interaction. Spectra of much higher resolution (<1 cm^{-1}) would be necessary to evaluate ϵ_1, ϵ_2, and ω_5 accurately.

In the spectrum of $C_2D_2^+$, a more intense feature appears on top of the Renner–Teller multiplets in combination with the ν_2 stretch. The Petelin–Kiselev model for Renner–Teller interaction does not include further complications due to Fermi resonances. The $C_2D_2^+$ features at ionization potentials of 11.724(5), 11.925(5), and 12.125(5) eV are proposed to originate from the ν_1 stretch, here evaluated at 2572(16) cm^{-1}. The unexpected enhancement of intensity may arise from interaction with the isoenergetic multiplet.

Correlation functions for the ground state of each ion are given in Fig. 4. In both cases substantial correlation is retained at longer times, indicative of the bound and stable electronic state. After one ν_2 vibrational period, 18.2 fs for $C_2H_2^+$ and 20.2 fs for $C_2D_2^+$, the correlation functions reach reduced values of 0.88 and 0.84, respectively. This initial loss is due to the dephasing of the high and low frequency oscillators comprising the wave packet. This phase relationship is responsible for weakly modulating the correlation function, and together with the vibrational anharmonicity serves to damp the correlation at longer times.

It is interesting to note that although the isotopic species possess similar anharmonicities and the heavier species is associated with longer periods, the correlation function for $C_2D_2^+$ decays more quickly. Several factors may contribute to this effect. One is that the proposed Fermi resonance for $C_2D_2^+$ may more effectively mix the near resonant modes, creating a phase randomization and loss of correlation. A second is that the vibrational wave packet for the heavier species is contracted in some dimensions of phase space and in the time-dependent picture $\phi(0)$ becomes a smaller target for the grazing incidence of $\phi(t)$.[25] A third is that the trajectory of the wave packet will be modified by the isotope effect, again influencing the incidence of $\phi(0)$ and $\phi(t)$. The experimental autocorrelation functions unfortunately cannot distinguish among these three effects.

B. $\tilde{A}\,^2A_g$ state

The isolated spectra of the first electronically excited state of $C_2H_2^+$ and $C_2D_2^+$ are presented in Fig. 5. Two

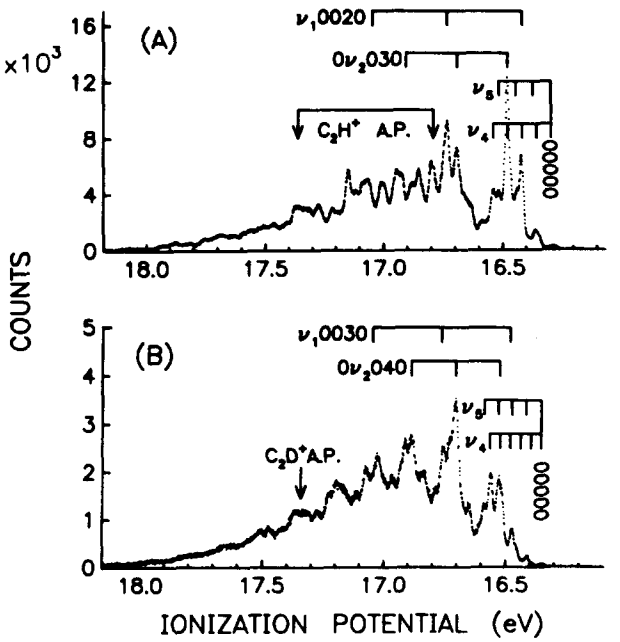

FIG. 5. The $\tilde{A}\,^2A_g$ state photoelectron bands of C_2H_2 (A) and C_2D_2 (B). Here ν_4 and ν_5 refer to the principal vibrational progressions in those normal modes, originating from the [00000] level. The appearance potential (A.P.) for C_2H^+ is indicated by a double arrow, designating both the low intensity threshold reported in Ref. 11 and the more intense step in ion yield at 17.36 eV. The appearance potential for C_2D^+ is obtained from Ref. 9.

strongly excited low frequency bending progressions indicate a nonlinear equilibrium geometry for this state. Temperature-dependent studies of $C_2H_2^+$ revealed dominant hot band contributions from ν_4, the *trans*-bending mode. A C_{2h} geometry is assigned to the $\tilde{A}\,^2\Sigma_g^+$ state on the basis of Franck–Condon considerations. The term symbol appropriate for this electronic state under C_{2h} symmetry is ^2A_g, rather than the traditional $^2\Sigma_g^+$ applied under an assumed $D_{\infty h}$ symmetry. The $\tilde{A}\,^2A_g$ term symbol will be adopted for this discussion.

An accurate evaluation of the adiabatic ionization potential is hindered by the negligible Franck–Condon overlap for the [00000] ← [00000] transition. Small peaks occurring at 16.297(5) eV for $C_2H_2^+$ and 16.351(5) for $C_2D_2^+$ are assigned to the adiabatic transitions, because no peaks comprising the progressions are observed at lower binding energies on a semilogarithmic scale. The 54 meV difference in adiabatic ionization potential between the two isotopic species is attributed to zero point energy differences. Another possibility, however, is that the true adiabatic transition is too weak to be detected by this experiment. The presently reported values may be conservatively regarded as upper bounds on the adiabatic ionization potentials for the $\tilde{A}\,^2A_g$ state.

In the threshold region the vibrational levels are sufficiently resolved to distinguish two low frequency progressions. The more intense progression is assigned to ν_4, which possesses the larger Franck–Condon overlap for a $C_{2h} \leftarrow D_{\infty h}$ change in geometry. The frequency of this mode is 492(12) cm^{-1} for $C_2H_2^+$ and 339(12) cm^{-1} for $C_2D_2^+$. The remaining low frequency mode is tentatively assigned to ν_{5B}, an in-plane *cis* bend. The frequency of ν_{5B} is thereby given as 605(12) cm^{-1} for $C_2H_2^+$ and 516(12) cm^{-1} for $C_2D_2^+$. The other possible assignment, ν_{5A}, is an out-of-plane *cis* bend, which would presumably be of lower intensity.

The vibrational manifold becomes extremely dense for the $\tilde{A}\,^2A_g$ state ions with vibrational internal energies greater than 0.20 eV. This is partially due to the onset of combination levels involving ν_4 and ν_{5B} and the two symmetry-allowed high frequency stretches, ν_1 and ν_2. Poor Franck–Condon overlaps for $[0\nu_2000] \leftarrow [00000]$ and $[\nu_1 0000] \leftarrow [00000]$ transitions make it difficult to evaluate the pure ν_1 and ν_2 frequencies accurately.

In order to determine ν_1 and ν_2, therefore, a simulation of the vibrational manifold of this photoelectron band was performed for each ion. This was accomplished by first simulating the threshold region of each spectrum with two low frequency progressions. The energies and relative intensities of the vibrational levels were obtained from the recorded spectra. Twelve meV Gaussians, corresponding to the instrumental resolution, were then convoluted with the stick spectra. Energies and intensities were adjusted to optimize the simulation of the recorded spectra in the threshold region. The high frequency modes were then combined with the low frequency mode progressions, without altering the relative intensity patterns of the low frequency modes. The ν_1 and ν_2 frequencies were adjusted, assuming $\nu_1 > \nu_2$, to generate a band shape comparable to the measured photoelectron bands. By this procedure ν_1 and ν_2 for $C_2H_2^+$ were evaluated at 2530(20) and 1730(20) cm^{-1}, respectively. For $C_2D_2^+$ ν_1 and ν_2 were found to be 2280(20) and 1450(20) cm^{-1}, respectively.

The simulated spectra display the general band shapes of the recorded spectra, as shown for each ion in Fig. 6. The intensity variations are largely credited to the assumptions used to assign peak intensities. Although the general band

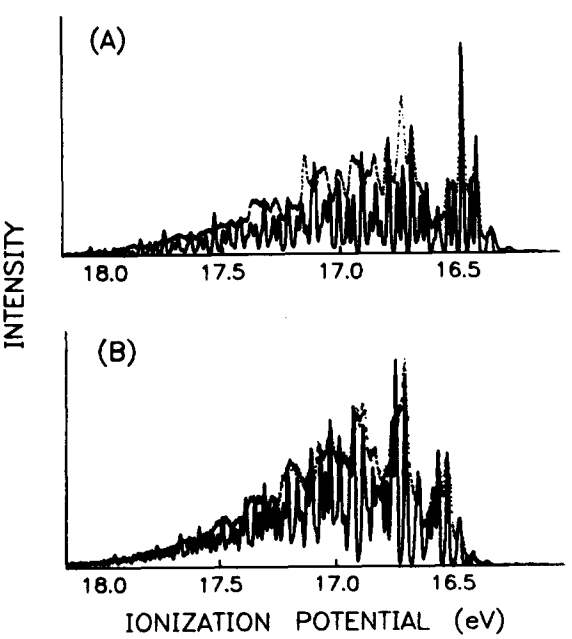

FIG. 6. A simulation of the vibrational manifold (line) is compared to the recorded photoelectron band (dots) for the $\tilde{A}\,^2A_g$ state of $C_2H_2^+$ (A) and $C_2D_2^+$ (B).

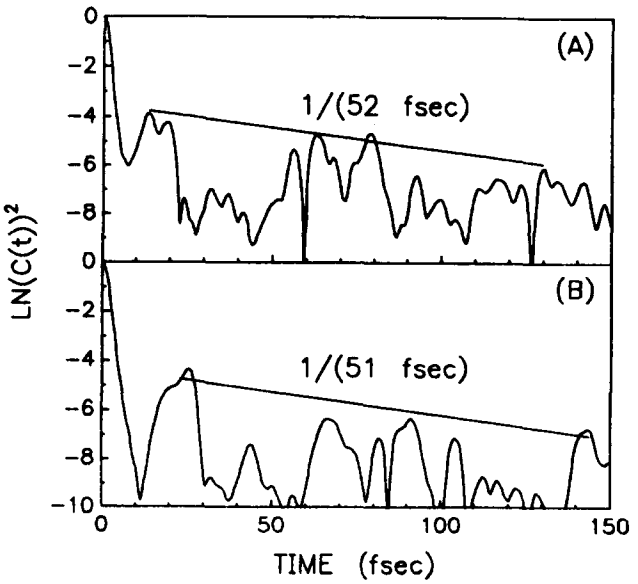

FIG. 7. The correlation functions derived for the $\tilde{A}\,^2A_g$ state of each species exhibits rapid decay, as indicated by the slope of $\ln\{[C(t)]^2\}$ shown for $C_2H_2^+$ (A) and $C_2D_2^+$ (B).

contours are similar, however, the density of states and linewidths are signficantly greater in the experimental spectra. The simple normal mode model appears to describe the complex photoelectron band inadequately. Even the vibrational levels near the bottom of the potential well are broadened significantly beyond the instrumental resolution. Spectra taken with a nozzle temperature of -62 °C show that this is not simply due to thermal broadening. Such line broadening and level density effects may be related to the stability of the $\tilde{A}\,^2A_g$ state.

The complex photoelectron band for the $\tilde{A}\,^2A_g$ state, the $C_{2h} \leftarrow D_{\infty h}$ change in geometry, the absence of any detectable $\tilde{A} \rightarrow \tilde{X}$ emission, and the delay of 0.5 eV above thermochemical threshold before appreciable C_2H^+ is formed suggest very interesting dynamics for the $\tilde{A}\,^2A_g$ state relaxation. The correlation functions exhibit an ultrafast decay, which has not been amenable to measurement by other methods. In order to ensure that the presence of hot bending modes in the spectrum did not appreciably alter the correlation functions, these functions were also determined for the acetylene spectrum taken at 120 °C and for the room temperature spectrum with an assumed Boltzmann distribution subtracted. The hot bands did not affect the results significantly.

Because the low frequency modes are heavily populated in the transition to the *trans*-bent state, a pronounced dephasing is evident in the correlation function at shorter times for each isotopic species. Following this initial dephasing, a correlation of 0.145 is achieved for $C_2H_2^+$ at 13 fs and 0.12 is achieved for $C_2D_2^+$ at 25 fs. Subsequent to the initial dephasing, the decay may be evaluated qualitatively from the slope of $\ln\{[C(t)]^2\}$, which is shown for each ion in Fig. 7. The decay time for each ion (51 fs for $C_2H_2^+$ and 52 fs for $C_2D_2^+$) is within one period of low frequency bending motion. No strong isotope effect is manifested beyond the deeper minima of the correlation function for the deuterated species. The $\tilde{A}\,^2A_g$ state relaxation therefore occurs on a 10^{-14} s time scale.

The correlation functions indicate the importance of the low frequency bending modes in the relaxation of the first electronically excited state. The photoelectron spectra had shown that these modes are populated extensively in combination with other symmetric stretching modes. The present results support the calculations of Rosmus, Botschwina, and Maier. Both the *trans*-bent geometry of this state and the strongly excited bending modes can initiate their proposed rearrangement to the $\tilde{A}\,^2A_g$ vinylidenic state. The autocorrelation functions further suggest that this relaxation pathway is irreversible, occurring in less than one period of bending motion.

C. $\tilde{B}\,^2\Sigma_u^+$ state

The principal peaks of the $\tilde{B}\,^2\Sigma_u^+$ state vibrational progressions were first observed and assigned by Baker and Turner.[5] For this electronic state $\nu_2 > \nu_1$, as a result of the C–C antibonding and C–H bonding character of the $2\sigma_u$ electron removed. The spectra presented in Fig. 8 exhibit more extensive vibrational progressions than were previously evident. Closer inspection of the individual levels, particularly the well isolated lower ionization potential features, reveals lines of very irregular profiles. Such peaks are inadequately described as single vibrational levels. The absence of any low frequency modes in the spectra indicates a linear geometry, which in turn signifies very small rotational constants for this state. The broad asymmetric peak shapes of the "vibrational" lines cannot, therefore, result from a rotational distribution. The temperature insensitivity of these features corroborates this conclusion. By ignoring the line profiles and evaluating the vibrational frequencies from the spacings between peak centroids, we arrive at frequencies of $\nu_1 = 1815(20)$ cm^{-1} and $\nu_2 = 2500(20)$ cm^{-1} for $C_2H_2^+$ and $\nu_1 = 1475(20)$ cm^{-1} and $\nu_2 = 2275(20)$ cm^{-1} for

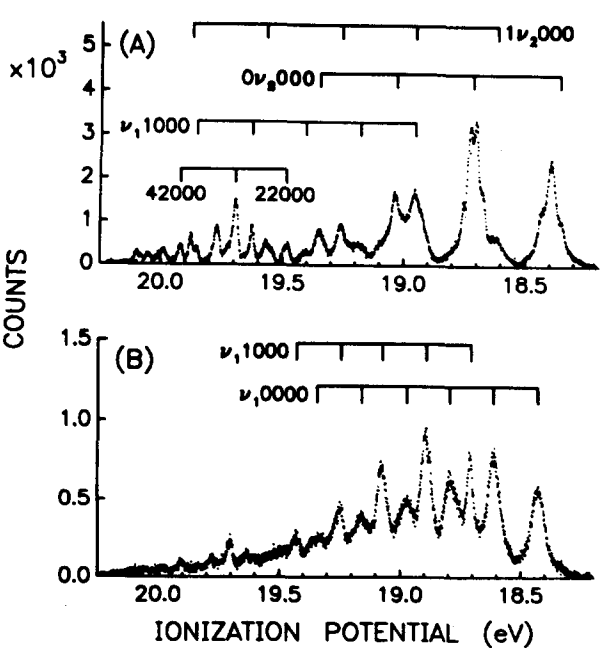

FIG. 8. The $\tilde{B}\,^2\Sigma_u^+$ state photoelectron bands of $C_2H_2^+$ (A) and $C_2D_2^+$ (B). The vibrational levels are determined from peak centroids.

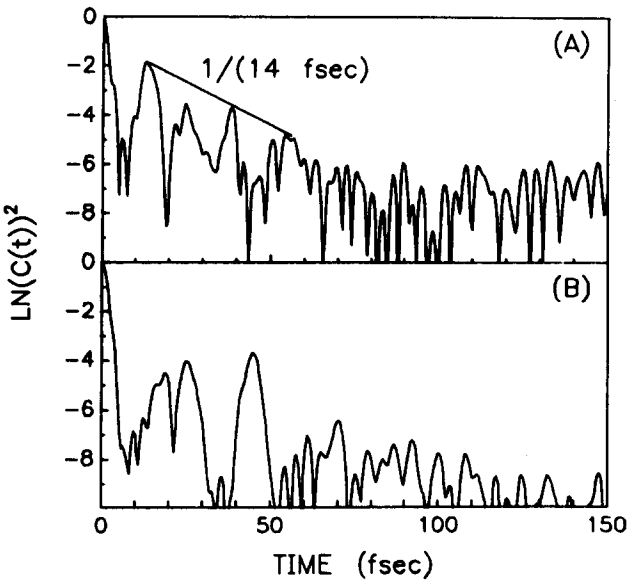

FIG. 9. The decay of the correlation functions derived from the $\tilde{B}\,^2\Sigma_u^+$ state of each species is demonstrated by the slope of $\ln\{[C(t)]^2\}$ for $C_2H_2^+$ (A) and $C_2D_2^+$ (B).

$C_2D_2^+$. Despite the irregular profiles of the individual peaks the levels follow a reasonably harmonic progression.

A comparison of the $C_2H_2^+$ and $C_2D_2^+$ $\tilde{B}\,^2\Sigma_u^+$ photoelectron spectra reveals their pronounced differences in band contours and vibronic line shapes. These differences do not result primarily from a variation in the initially prepared ensemble of states, but from the subsequent behavior of the two ensembles. The erratic line shapes and the magnitude of the splitting of the $C_2H_2^+$ [00000] and [01000] levels suggests that a vibronic coupling mechanism is operative. The large isotope effect demonstrates the strength of this vibronic perturbation, which is determined by the nuclear kinetic energy operators coupling the $\tilde{B}\,^2\Sigma_u^+$ state vibronic levels to those of a nearby potential energy surface. Köppel, Domcke, and Cederbaum have theoretically treated the coupling of two potential energy surfaces for molecular ions by multimode vibronic interaction.[26] Using the $\tilde{A}$ and $\tilde{X}$ states of $C_2H_4^+$ as an example, they demonstrate that two surfaces can couple with sufficient strength to obviate an application of the Born–Oppenheimer approximation. This coupling can lead to a splitting and shifting of spectral features, resulting in a dense and irregular photoelectron band. In the case of $C_2H_2^+$ and $C_2D_2^+$, the $\tilde{B}\,^2\Sigma_u^+$ surface may couple to the nearby $\tilde{A}\,^2A_g$ surface. Energy proximity is not a prerequisite to multimode vibronic coupling,[26] however, and a vibronic coupling to the ground state potential energy surface must also be considered.

The correlation functions for the $\tilde{B}\,^2\Sigma_u^+$ state of each ion were evaluated. Following the initial wave packet dephasing, reduced maxima are reached for $C_2H_2^+$ (0.35 at 13 fs) and $C_2D_2^+$ (0.12 at 15 fs). The $C_2H_2^+$ correlation function continues to decay rapidly, as demonstrated by the slope of $\ln\{[C(t)]^2\}$, presented in Fig. 9 for each ion. The slope of $\ln\{[C(t)]^2\}$ yields a decay time of 14 fs for this state of $C_2H_2^+$. This 14 fs decay time indicates that relaxation is occurring on the order of a single period of symmetric stretching motion. The correlation function for $C_2D_2^+$ exhibits the same relaxation behavior, but at shorter time a complex beating pattern reduces the value to 0.12, preventing an evaluation of the decay time from the slope of this species.

Two ultrafast decay mechanisms may be suggested for the $\tilde{B}\,^2\Sigma_u^+$ state. One is through a spin-orbit coupling to the repulsive $^4\Pi_u$ state, as originally suggested by Fiquet-Fayard. Another, as discussed above, is through a vibronic coupling to a lower potential energy surface ($\tilde{A}\,^2A_g$ or $\tilde{X}\,^2\Pi_u$). The spectroscopic differences that distinguish the $C_2H_2^+$ and $C_2D_2^+$ photoelectron bands indicate that the latter mechanism is more important. The spin-orbit coupling cannot account for the erratic vibronic line shapes and the pronounced isotope effect. A definitive interpretation of the relaxation of this state warrants a theoretical treatment.

V. CONCLUSION

Rotationally cold photoelectron spectra of C_2H_2 and C_2D_2 of improved resolution have allowed each of the three electronic states accessible with HeI radiation to be characterized in greater detail. For the $\tilde{X}\,^2\Pi_u$ state the ν_4 bending vibration was evaluated and the ν_5 origin of the Renner–Teller was identified. Enhanced intensity of the Renner–Teller multiplet in combination with ν_2 for $C_2D_2^+$ may be explained by a Fermi resonance with the ν_1 stretch. The *trans*-bent geometry of the $\tilde{A}\,^2A_g$ state could be determined from the previously unobserved low frequency ν_4 and ν_{5B} vibrational progressions, and refined ν_1 and ν_2 frequencies were obtained from spectral simulations. An extended vibrational progression was found for the $\tilde{B}\,^2\Sigma_u^+$ state. Although these levels followed a reasonable harmonic progression, the irregular line profiles indicated strong nonadiabatic effects.

Correlation functions for all three electronic states were derived. Variations between the isotopic species' correlation functions were attributed primarily to differences in the phase space spanned by the initially formed wave packets. Ultrafast decay mechanisms were evident for the $\tilde{A}\,^2A_g$ and $\tilde{B}\,^2\Sigma_u^+$ states of each ion. The decay of the first excited $\tilde{A}\,^2A_g$ state occured in less than one period of bending vibration, supporting the relaxation pathway through a vinylidene ion intermediate as proposed by Rosmus, Botschwina, and Maier. The decay of the $\tilde{B}\,^2\Sigma_u^+$ state was the more rapid, occurring in less than 14 fs for $C_2H_2^+$. A vibronic coupling mechanism involving the lower potential energy surfaces of the ions may explain this rapid decay. The experimentally derived correlation functions corroborate earlier experimental investigations which noted the absence of radiation from the excited state acetylene ion.

ACKNOWLEDGMENTS

This work was supported by the Director, Office of Energy Research, Office of Basic Energy Sciences, Chemical Sciences Division of the U.S. Department of Energy under Contract No. DE-AC03-76SF00098.

[1] E. J. Heller, Acc. Chem. Res. **14**, 368 (1981), and references therein.
[2] A. J. Lorquet, J. C. Lorquet, J. Delwiche, and M. J. Hubin-Franskin, J. Chem. Phys. **76**, 4692 (1982).

[3]J. E. Pollard, D. J. Trevor, J. E. Reutt, Y. T. Lee, and D. A. Shirley, J. Chem. Phys. **81**, 5302 (1984).
[4]H. Köppel, Chem. Phys. **77**, 359 (1983).
[5]C. Baker and D. W. Turner, Proc. R. Soc. London Ser. A **308**, 19 (1968).
[6]R. G. Cavell and D. A. Allison, J. Chem. Phys. **69**, 159 (1978).
[7]P. M. Dehmer and J. L. Dehmer, J. Electron. Spectrosc. Relat. Phenom. **28**, 145 (1982).
[8]T. Hayaishi, S. Iwata, M. Sasanuma, E. Ishiguro, Y. Morioka, Y. Iida, and M. Nakamora, J. Phys. B **15**, 79 (1982).
[9]R. Botter, V. H. Dibeler, J. A. Walker, and H. M. Rosenstock, J. Chem. Phys. **44**, 1271 (1966).
[10]V. H. Dibeler, J. A. Walker, and K. E. McCulloh, J. Chem. Phys. **59**, 2264 (1973).
[11]Y. Ono and C. Y. Ng, J. Chem Phys. **74**, 6985 (1981).
[12]J. H. D. Eland, Int. J. Mass. Spectrom. Ion Phys. **31**, 161 (1979).
[13]Unpublished work by M. Devoret and J. H. D. Eland cited in Ref. 12 by the method described in Chem. Phys. Lett. **43**, 97 (1976).
[14]P. C. Haarhoff, Mol. Phys. **8**, 49 (1964).
[15]Florence Fiquet-Fayard, J. Chim. Phys. **64**, 320 (1967).
[16]P. Rosmus, P. Botschwina, and J. P. Maier, Chem Phys. Lett. **84**, 71 (1981).
[17]J. E. Pollard, D. J. Trevor, Y. T. Lee, and D. A. Shirley, Rev. Sci. Instrum. **52**, 1837 (1981).
[18]P. R. Keller, D. Mehaffy, J. W. Tayler, F. A. Grimm, and T. A. Carlson, J. Electron. Spectrosc. Relat. Phenom. **27**, 223 (1982).
[19]A. Lofthus and P. H. Krupenie, J. Phys. Chem. Ref. Data **6**, 113 (1977).
[20]*Atomic Energy Levels*, Vols. I and III, edited by Charlotte E. Moore (National Bureau of Standards, Washington, D. C., 1958).
[21]S. V. O'Neil and W. P. Reinhardt, J. Chem. Phys. **69**, 2126 (1978).
[22]Gerhard Herzberg, *Molecular Spectra and Molecular Structure. III. Electronic Spectra & Electronic Structure of Polyatomic Molecules* (Van Nostrand Reinhold, New York, 1966).
[23]K. P. Huber and G. Herzberg, *Molecular Spectra and Molecular Structure. IV. Constants of Diatomic Molecules* (Van Nostrand Reinhold, New York, 1979).
[24]A. N. Petelin and A. A. Kiselev, Int. J. Quantum Chem. **6**, 701 (1972).
[25]E. J. Heller, in *Potential Energy Surfaces and Dynamics Calculations*, edited by D. Truhlar (Plenum, New York, 1981).
[26]H. Köppel, W. Domcke, and L. S. Cederbaum, Adv. Chem. Phys. **57**, 59 (1984).